

Molecular Probes for Imaging of Hypoxia in the Retina

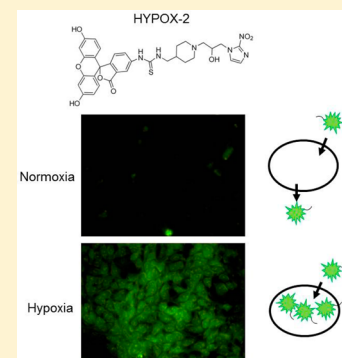
Stephanie M. Evans,[†] Kwangho Kim,[‡] Chauca E. Moore,[†] Md. Imam Uddin,[†] Megan E. Capozzi,[§] Jason R. Craft,[†] Gary A. Sulikowski,[‡] and Ashwath Jayagopal^{*,†,§}

[†]Department of Ophthalmology and Visual Sciences, Vanderbilt Eye Institute, Nashville, Tennessee 37232, United States

[‡]Departments of Chemistry and Biochemistry and [§]Department of Molecular Physiology and Biophysics, Vanderbilt University, Nashville, Tennessee 37235, United States

Supporting Information

ABSTRACT: Hypoxia has been associated with retinal diseases which lead the causes of irreversible vision loss, including diabetic retinopathy, retinopathy of prematurity, and age-related macular degeneration. Therefore, technologies for imaging hypoxia in the retina are needed for early disease detection, monitoring of disease progression, and assessment of therapeutic responses in the patient. Toward this goal, we developed two hypoxia-sensitive imaging agents based on nitroimidazoles which are capable of accumulating in hypoxic cells *in vivo*. 2-nitroimidazole or Pimonidazole was conjugated to fluorescent dyes to yield the imaging agents HYPOX-1 and HYPOX-2. Imaging agents were characterized in cell culture and animal models of retinal vascular diseases which exhibit hypoxia. Both HYPOX-1 and -2 were capable of detecting hypoxia in cell culture models with >10:1 signal-to-noise ratios without acute toxicity. Furthermore, intraocular administration of contrast agents in mouse models of retinal hypoxia enabled ex vivo detection of hypoxic tissue. These imaging agents are a promising step toward translation of hypoxia-sensitive molecular imaging agents in preclinical animal models and patients.



INTRODUCTION

The retina is supplied with oxygen by two separate vascular systems, the choroidal or outer retinal circulation, and the inner retinal circulation.¹ Adequate oxygen supply is critical for normal functioning of the retina. The high oxygen requirements of the retina for proper function and the unique structure required for light to reach the photoreceptors make it vulnerable to vascular diseases.² Hypoxia plays a role in the onset and progression of various retinal vascular diseases including diabetic retinopathy and age-related macular degeneration, both leading causes of irreversible blindness.^{3–5} Therefore, strategies to monitor hypoxia in cell culture and animal models of these diseases and patients are warranted.

Advancements in technologies including retinal oximetry, phosphorescence lifetime imaging, and Doppler optical coherence tomography (OCT) have provided a greater understanding of vascular oxygen supply and metabolism in the retina. Retinal oximetry measures vascular oxygen tension in inner retinal^{6–9} and choroidal vasculature¹⁰ based on hemoglobin oxygen saturation. Phosphorescence lifetime imaging measures oxygen levels using an oxygen sensitive agent that is quenched by oxygen allowing for vascular pO₂ levels to be quantified.¹¹ Doppler OCT measures retinal blood flow, which can be used to derive retinal oxygen metabolic measurements.¹² We seek to complement these approaches by developing hypoxia-sensitive contrast agents which enable visualization of hypoxic tissue in the retina and other tissues.

Our approach is based on the conjugation of fluorescing dyes to hypoxia-sensitive nitroimidazole moieties such as 2-nitro-

imidazole and Pimonidazole, which are known to accumulate within hypoxic cells.^{13–15} When injected *in vivo*, the nitro groups of these compounds are bioreduced by nitroreductases in hypoxic tissues (pO₂ < 10 mmHg), triggering formation of intracellular protein adducts.¹⁶ In traditional applications, detection of hypoxic tissue is carried out via antibody based immunohistochemical staining on excised tissues. We sought to develop a new synthetic route to conjugate fluorescent dyes to nitroimidazoles toward enabling longitudinal *in vivo* imaging applications which facilitate imaging of hypoxic tissue while obviating the tissue dissection and processing steps. We focused on development of clinically translatable imaging agents featuring FDA-approved fluorescein dyes, which are routinely used in ophthalmic examinations.

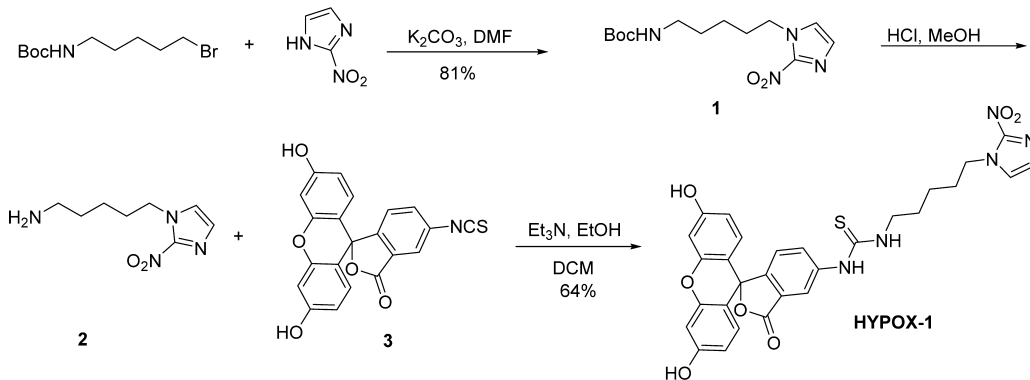
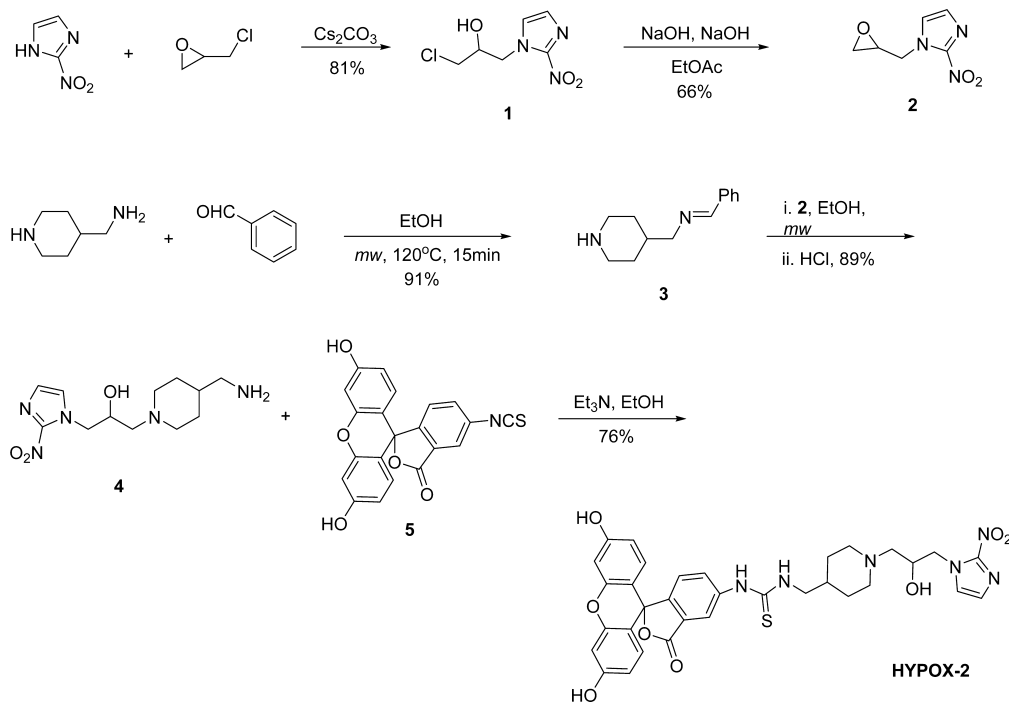
The goal of this work was to develop a hypoxia-sensitive imaging agent that would identify hypoxic cells in living tissue. To accomplish this, nitroimidazole derivatives were conjugated to fluorescein isothiocyanate (FITC) to create the imaging agents HYPOX-1, a 2-nitroimidazole containing reagent, and HYPOX-2, a Pimonidazole containing reagent. Established cell culture and mouse models of hypoxia-associated retinal disease were used to test the specificity of both imaging agents for hypoxic cells.

Received: August 26, 2014

Revised: September 22, 2014

Published: September 24, 2014



Scheme 1. Synthesis of HYPOX-1**Scheme 2. Synthesis of HYPOX-2**

■ RESULTS AND DISCUSSION

HYPOX-1 features a 2-nitroimidazole group coupled to FITC via a 6 carbon linkage (Scheme 1). Similarly, synthesis of HYPOX-2 was carried out to yield a FITC dye attached directly to amine-activated Pimonidazole (Scheme 2). Yields were 64% (HYPOX-1) and 76% (HYPOX-2), and compounds were characterized using LC/MS and NMR analysis (Supporting Information Figures 1–4).

In order to measure the specificity of HYPOX-1 and HYPOX-2 for hypoxic retinal tissues *in vitro*, R28 rat retinal neuronal cells^{17,18} or primary human Müller cells¹⁹ were conditioned in a hypoxic chamber purged with a mixture of nitrogen/carbon dioxide up to 12 h. These two cell lines model predominantly oxygen-sensitive cell types in retinal diseases with a hypoxia-ischemia component.²⁰ We confirmed that hypoxia was achieved in retinal cell lines using Pimonidazole adduct immunostaining (Supporting Information Figure 5) and qRT-PCR analysis of the hypoxia-specific biomarker carbonic anhydrase II (Supporting Information Figure 6).²¹ In a microplate fluorescence spectrophotometric assay (Figure

1A–D), hypoxia-conditioned R28 cells and human Müller cells exhibited significantly higher fluorescence intensity than normoxia-conditioned R28 cells and human Müller cells when treated with HYPOX-1 and HYPOX-2. The micromolar doses of HYPOX-1 and HYPOX-2 used in these experiments are modeled on doses used to achieve optimal signal to background ratios using Pimonidazole immunohistochemistry.²² At the concentration of Pimonidazole typically used for immunohistochemical assays (100 μ M), HYPOX-1 and -2 fluorescence emission was 2.7- and 4.4-fold higher in hypoxic R28 cells vs normoxic R28 cells, with enhanced signal-to-noise ratios observed for the 50 μ M dose (Figure 1A,B). HYPOX-1 and HYPOX-2 showed 5-fold and 11-fold increases in hypoxic/normoxic fluorescence intensity ratios, respectively, in human Müller cells (Figure 1C,D). At concentrations lower than 50 μ M, HYPOX-1 was not detectable. However, HYPOX-2 was effective at 10 μ M in human Müller cells showing a 32-fold greater fluorescence intensity in hypoxia-conditioned cells (Figure 1D). These data demonstrate that HYPOX-1 and -2 are selectively retained in hypoxic retinal cells irrespective of cell type and species origin.

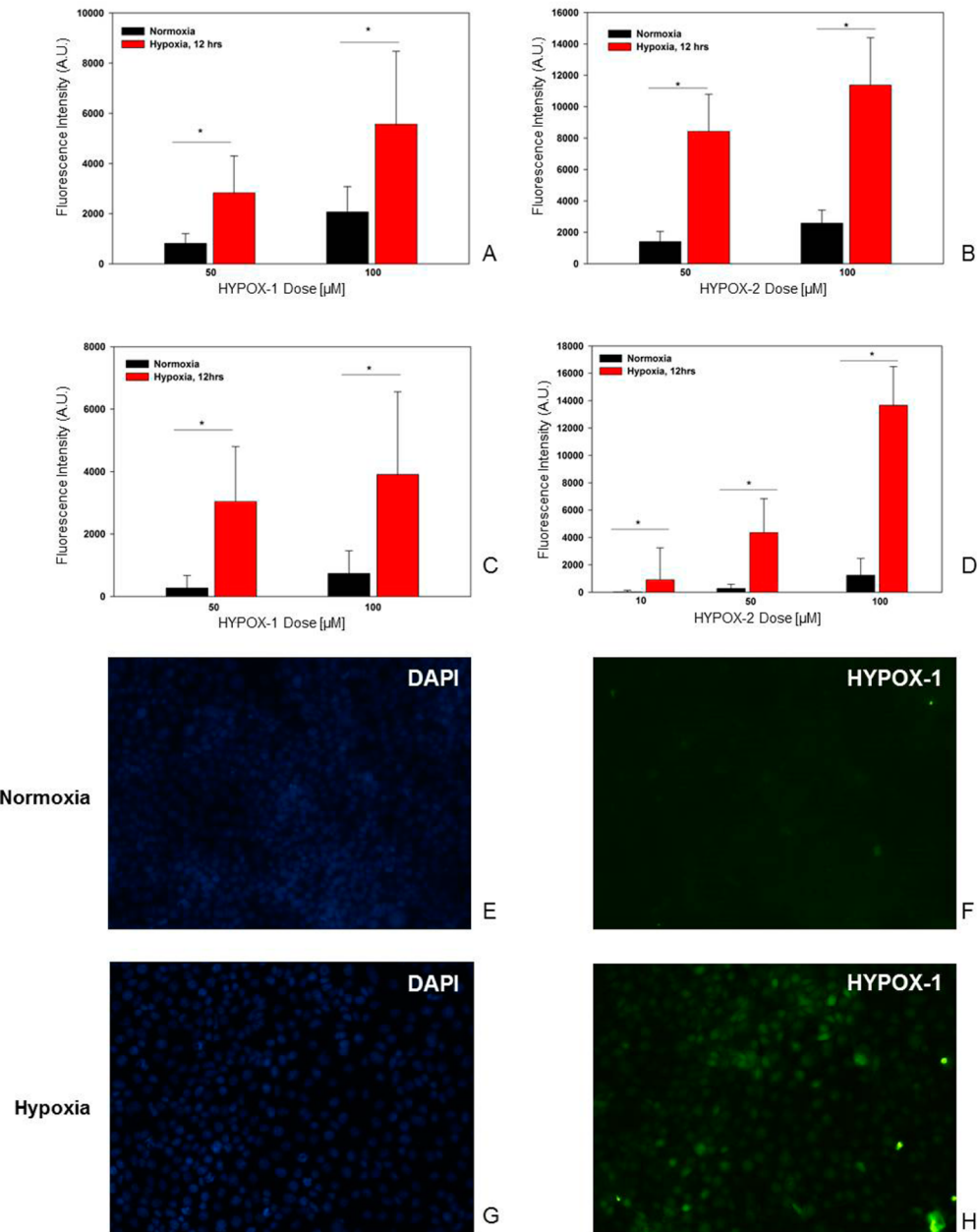


Figure 1. Hypoxic R28 and Müller cells treated with HYPOX imaging agents exhibit dose-dependent fluorescence enhancement in a microplate fluorescence spectrophotometric assay. Cells were conditioned under normoxic conditions or 12 h of hypoxia. (A-B) HYPOX-1 and HYPOX-2 treated R28 cell assay. (C-D) HYPOX-1 and HYPOX-2 treated Müller cell assay. ($n = 8$) * $p < 0.01$. R28 cells were treated with 100 μ M HYPOX-1 (green) and (E-F) normoxia or (G-H) hypoxia-conditioned for 4 h and stained with DAPI (blue).

Fluorescence microscopy of R28 cells treated with HYPOX-1 and -2 confirmed observations in microplate spectrophotometry assays (Figures 1E–H and 2). Furthermore, hypoxic cells incubated with HYPOX-1 and -2, but not normoxic cells, were positive for Pimonidazole adducts as detectable by an adduct-specific antibody (Hypoxyprobe) which does not bind to Pimonidazole moieties alone (Figure 2F). These results were further confirmed by Western Blot analysis, in which hypoxic and normoxic cell lysates were probed with a Hypoxyprobe antibody (Supporting Information Figure 7). These data suggest that HYPOX-1 and -2 accumulate in hypoxic cells by the same bioreduction/adduct formation mechanism observed for nitroimidazole compounds.¹⁴

Both imaging agents were not acutely toxic to retinal cells as assessed by BrdU cell proliferation assays (Figure 3A,B). Cells exposed to up to 100 μ M of HYPOX-1 or HYPOX-2 showed no significant decrease in cell proliferation, indicating that these agents do not interfere with cell cycle and are safe at these concentrations. Furthermore, TUNEL assays on retinas from mice intravitreally injected with HYPOX-1 did not exhibit acute toxicity as indicated by lack of TUNEL positive cells (Figure 3C). These data confirm the safety of the HYPOX components, fluorescein and nitroimidazoles, which have been administered to patients for decades without associated toxicity.^{16,23,24}

In order to demonstrate the *in vivo* hypoxia selectivity of these imaging agents in the retina, HYPOX-1 and HYPOX-2 were administered to mouse models of oxygen-induced

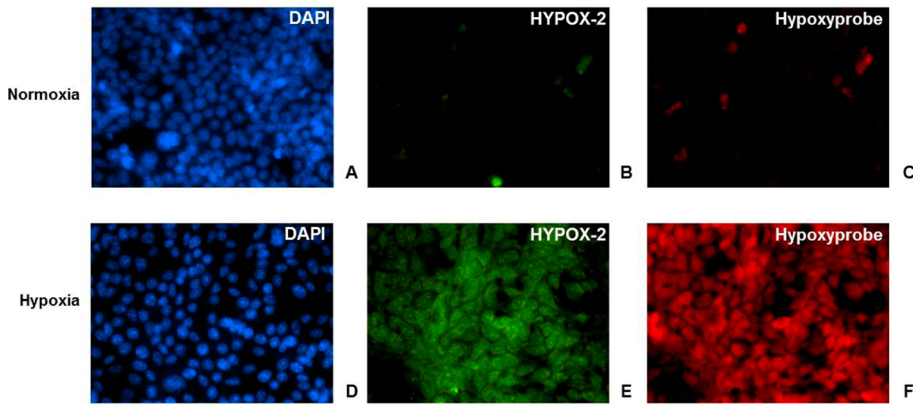


Figure 2. R28 retinal neuronal cell lines conditioned under (A–C) normoxic or (D–F) hypoxic (4 h) conditions were incubated with 100 μ M HYPOX-2 (green) followed by fixation and immunostaining with an antibody specific for Pimonidazole adducts, Hypoxyprobe, (red) in hypoxic cells.

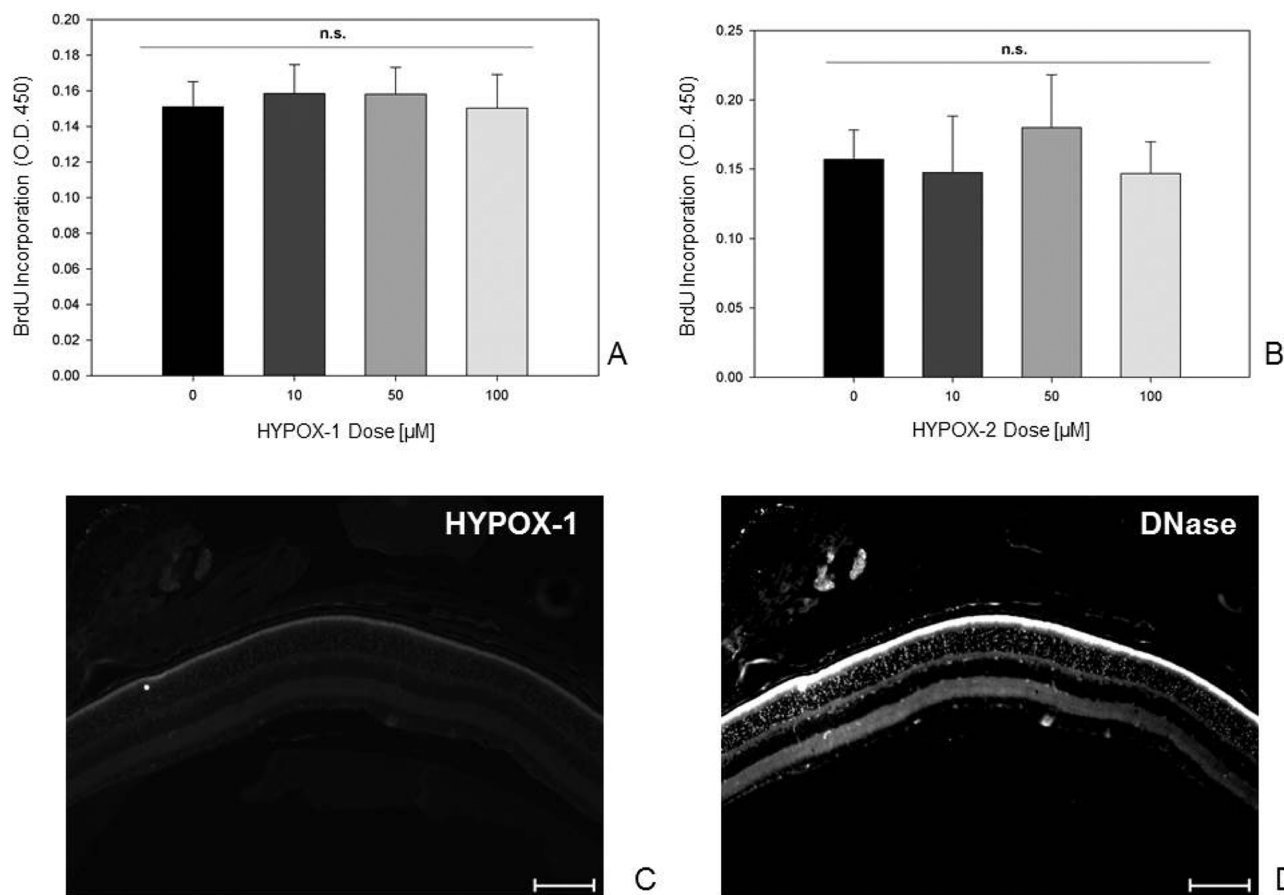


Figure 3. R28 cells treated with (A) HYPOX-1 or (B) HYPOX-2 for 24 h show no significant decrease in cell proliferation as indicated by a BrdU incorporation assay. ($n = 4$), $p < 0.01$. (C,D) A TUNEL assay was performed on cross sections of retinas from adult C57BL/6 mice: (C) HYPOX-1 treated retina exhibits only autofluorescence of the retinal pigmented epithelium (RPE) and lack of TUNEL staining; (D) DNase treated cross sections were used as a TUNEL-positive control. Scale bars = 100 μ M.

retinopathy (OIR), which develop avascular, hypoxic central retinas on P13 and are used to model ischemic retinopathies observed in patients.^{25,26} Representative ex vivo imaging of dissected retinal flatmounts from OIR mice exhibited accumulation of intravitreally injected HYPOX-1 in central avascular retinas which are hypoxic in these animals, as confirmed by positive immunostaining for Pimonidazole adducts (Hypoxyprobe) in the same region (Figure 4A,B).

Intravitreally injected HYPOX-1 did not accumulate in age matched control mice, which develop fully vascularized retinas (Figure 4C), and lack of Pimonidazole adduct staining was also confirmed in these retinas (Figure 4D).

Immunostaining of excised retinas with ICAM-2 was used to identify retinal vasculature and its association with HYPOX-1 and -2 accumulation. As expected, intravenously or intravitreally injected HYPOX-1 or -2 accumulated in avascular

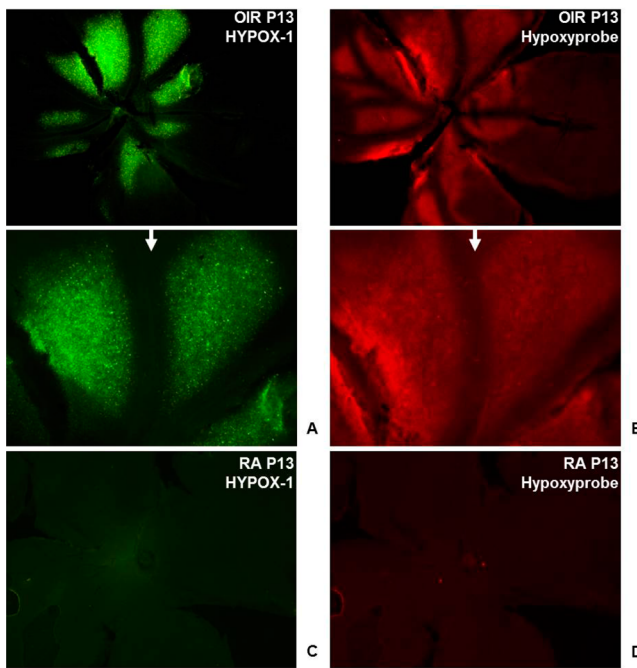


Figure 4. Retinal flatmounts of the OIR model, which features avascular hypoxic retina, exhibit colocalization of intravitreally administered HYPOX-1 and Pimonidazole. (A) HYPOX-1 in P13 OIR mouse retina. (B) Pimonidazole immunostaining colocalizes with HYPOX-1 in OIR P13 retinas. (C,D) Room air control mice which do not develop central avascular retinas and subsequent hypoxia exhibited no detectable HYPOX-1 accumulation or Pimonidazole staining.

regions not supplied by the ICAM-2 positive blood vessels (Figure 5A,C). Control mice reared in room air did not exhibit HYPOX-1 accumulation (Figure 5B). In some retinal regions in OIR mice, ICAM-2 positive blood vessels colocalized with HYPOX-1 or -2 fluorescence emission. These observations are consistent with published reports which indicate that blood vessels in the OIR mouse model on P12–P15 also exhibit some degree of hypoxia, since these fragile blood vessels are often not well-perfused and lack adequate oxygen carrying capacity.^{25,27} However, as these compounds are intravenously injected, it is possible that some intravascular trapping of HYPOX compounds may occur, which warrants further investigation. These data demonstrate the specificity of HYPOX probes for hypoxic tissue *in vivo*, and warrant further applications involving *in vivo* retinal imaging instrumentation. In addition, HYPOX accumulation in retinal tissue can be accomplished through intraocular or intravenous injection routes. We are currently designing instrumentation and protocols to enable

visualization of *in vivo* administered HYPOX-1 and -2 in mouse models of retinal hypoxia.

This work builds upon recently described approaches for imaging hypoxia in other organs in animal models.^{28–30} These innovative imaging probes enable detection of hypoxia in cells or tissues via FRET or nitroreductase bioreduction mechanisms. Our goal was to facilitate translation of hypoxia imaging for ophthalmic examination, as no hypoxia imaging agents have been tested in this setting. We have now contributed an additional imaging contrast agent which enables the coupling of the FDA-approved fluorescein to 2-nitroimidazole or Pimonidazole for selective imaging of hypoxic cells in the retina. Further work remains to compare the imaging agents described here and in the literature to optimize dosage and imaging protocols for each contrast agent in diverse imaging applications.

CONCLUSIONS

In this work we have demonstrated a facile route for synthesis of hypoxia-sensitive imaging agents based on biocompatible nitroimidazole and fluorescein components. The imaging probes were capable of detection of hypoxic retinal cells and tissues with high specificity and sensitivity. This approach may be useful for studying the role of hypoxia in retinal diseases, as well as diseases in other tissues featuring a hypoxic component. Further studies are warranted to demonstrate amenability of this approach for imaging hypoxia using *in vivo* imaging instrumentation in animal models and patients.

EXPERIMENTAL PROCEDURES

Materials. Human Müller cells were a gift of Dr. John Penn (Vanderbilt Eye Institute) and were purified and characterized as previously published.¹⁹ R28 rat retinal neuronal cells¹⁸ were purchased from KeraFast. Human Retinal Microvascular Endothelial Cells (HRMEC) were purchased from Cell Systems. Low glucose DMEM, Fetal Bovine Serum, GlutaMax, and Penicillin–Streptomycin were obtained from GIBCO. Endothelial Cell Media (EBM) and EGM SingleQuots Kit were purchased from Lonza. BrdU Cell Proliferation assay kit was obtained from Exalpha Biologicals. A Billups-Rothenberg chamber was used for hypoxia induction. Hypoxyprobe antibody was purchased from Hypoxyprobe Inc. TUNEL Fluorimetric detection kit, Alexa Fluor 647 (AF647) secondary donkey anti-rabbit antibody and Prolong Gold mounting media with DAPI were purchased from Life Technologies. Details regarding characterization of HYPOX-1 and HYPOX-2 are described in the Supporting Information.

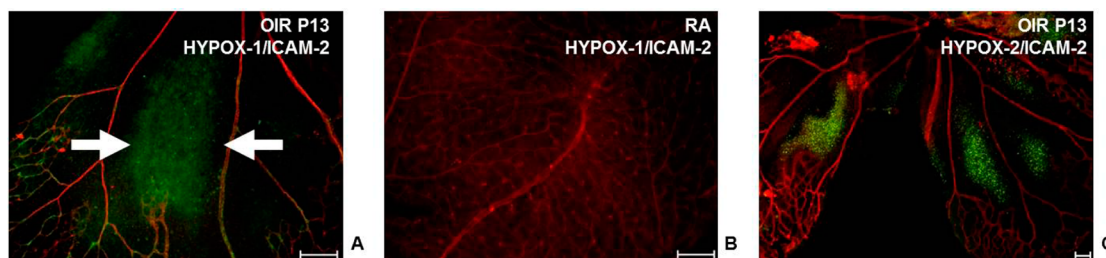


Figure 5. Retinal flatmounts from (A) OIR or (B) room air mice intravenously injected with HYPOX-1 (green) were stained with the endothelial cell marker ICAM-2 (red). (C) Retinal flatmount from OIR mouse intravitreally injected with HYPOX-2 (green) and stained with ICAM-2 (red). Accumulation of HYPOX-1 and HYPOX-2 is observed in the avascular retina. Scale bars = 100 μ M.

Synthesis of HYPOX-1. *tert*-Butyl (5-(2-nitro-1*H*-imidazol-1-yl)pentyl)carbamate 1. To a solution of 2-nitroimidazole (51 mg, 0.45 mmol) and *tert*-butyl (5-bromopentyl)carbamate (100 mg, 0.38 mmol) in DMF (3.5 mL), potassium carbonate (79 mg, 0.57 mmol) was added. The reaction mixture was heated at 80 °C for 20 min under microwave then cooled to room temperature, filtered through a Celite pad, and the filtrate concentrated in vacuo. The residue was purified by column chromatography using Hex/EtOAc (gradient: 0 to 50% EtOAc) to afford *tert*-butyl (5-(2-nitro-1*H*-imidazol-1-yl)pentyl)carbamate 1 (92 mg, 81%) as an oil. ¹H NMR (CDCl₃, 400 MHz) δ (ppm) 7.14 (s, 1H), 7.08 (s, 1H), 4.41 (t, J = 7.2 Hz, 2H), 3.14–3.10 (m, 2H), 1.88 (qt, J = 7.6 Hz, 2H), 1.60–1.48 (m, 2H), 1.44 (s, 9H), 1.40–1.31 (m, 2H); LCMS (ESI) tR: 0.906 min (>99%, ELSD), m/z: 299.3 [M+1]⁺.

5-(2-Nitro-1*H*-imidazol-1-yl)pentan-1-amine 2. To a solution of compound 1 (143 mg, 0.48 mmol) in MeOH (5 mL), HCl (0.8 mL, 1.2 N solution) was added at room temperature. The reaction mixture was stirred for 5 h and solvent was removed in vacuo. The residue was washed with dichloromethane (3 × 20 mL) to afford 5-(2-nitro-1*H*-imidazol-1-yl)pentan-1-amine 2 (111 mg, 99%) as white solid. ¹H NMR (MeOD, 400 MHz) δ (ppm) 7.54 (s, 1H), 7.18 (s, 1H), 4.52 (t, J = 7.2 Hz, 2H), 2.96 (t, J = 7.6 Hz, 2H), 1.95 (qt, J = 7.6 Hz, 2H), 1.74 (qt, J = 7.6 Hz, 2H), 1.49 (qt, J = 8.0 Hz, 2H); LCMS (ESI) tR: 0.082 min (>99%, ELSD), m/z: 284.16 [M+1]⁺.

HYPOX-1. To a solution of compound 2 (35 mg, 0.15 mmol) in MeOH/dichloromethane (1/2 mL), triethylamine (42 μL, 0.3 mmol) was added followed by adding Fluorescein isothiocyanate 3 (58 mg, 0.15 mmol). The reaction mixture was heated at 80 °C for 15 min under microwave then cooled to room temperature and concentrated in vacuo. The residue was purified by column chromatography using dichloromethane/MeOH (gradient: 0 to 50% MeOH) to provide HYPOX-1 (55 mg, 64%) as yellow solid. ¹H NMR (MeOD, 400 MHz) δ (ppm) 8.09 (d, J = 1.6 Hz, 1H), 7.74 (d, J = 8.0 Hz, 1H), 7.53 (d, J = 0.8 Hz, 1H), 7.18 (d, J = 8.4 Hz, 1H), 7.15 (d, J = 0.8 Hz, 1H), 6.77 (d, J = 8.8 Hz, 2H), 6.69 (d, J = 2.4 Hz, 2H), 6.57 (dd, J = 2.4, 8.4 Hz, 2H), 4.52 (t, J = 7.2 Hz, 2H), 3.70–3.60 (m, 2H), 1.96 (qt, J = 7.2 Hz, 2H), 1.74 (qt, J = 7.2 Hz, 2H), 1.49 (qt, J = 7.2 Hz, 2H); LCMS (ESI) tR: 0.756 min (>99%, ELSD), m/z: 673.1 [M+1]⁺.

Synthesis of HYPOX-2. 2-Nitro-1-(oxiran-2-ylmethyl)-1*H*-imidazole 2. A mixture of 2-nitroimidazole (250 mg, 2.21 mmol), epichlorohydrin (5 mL), and potassium carbonate (31 mg, 0.22 mmol) was heated under reflux condition for 20 min. The yellow 1-chloro-3-(2-nitro-1*H*-imidazol-1-yl)propan-2-ol 1 was collected by filtration and then dissolved in mixture of ethyl acetate (5 mL) and sodium hydroxide (5 mL, 2 M solution). The reaction mixture was stirred for 1 h at room temperature and extracted with ethyl acetate (3 × 5 mL), and then the organic layer was dried over MgSO₄. The residue was purified by column chromatography using dichloromethane/MeOH (gradient: 0 to 10% MeOH) to provide white solid 2-nitro-1-(oxiran-2-ylmethyl)-1*H*-imidazole 2. (300 mg, 66%).

(E)-N-Benzylidene-1-(piperidin-4-yl)methanamine 3. A mixture of piperidin-4-ylmethanamine (1.48 mL, 12.3 mmol) and benzaldehyde (1.28 mL, 12.3 mmol) in ethanol (9.4 mL) was heated at 120 °C for 15 min under microwave condition then solvent was removed in vacuo to give (E)-N-benzylidene-1-(piperidin-4-yl)methanamine 3 as a yellow oil (2.71 g, 91%) and used without further purification.

1-(4-(Aminomethyl)piperidin-1-yl)-3-(2-nitro-1*H*-imidazol-1-yl)propan-2-ol 4. A mixture of (E)-N-benzylidene-1-(piperidin-4-yl)methanamine 3 (310 mg, 1.54 mmol) and 2-nitro-1-(oxiran-2-ylmethyl)-1*H*-imidazole 2 (217 mg, 1.28 mmol) in ethanol (8 mL) was heated at 120 °C for 20 min under microwave condition then concentrated under reduced pressure. Two mL of HCl (1.2 N solution) was added to the resulting residue, and then the mixture was heated at 40 °C for 4 h. The reaction mixture was extracted with dichloromethane (4 × 8 mL). The aqueous layer was treated with 40% of NaOH solution to adjust pH 11 then extracted with dichloromethane (4 × 10 mL) to provide 4 as yellow oil (325 mg, 89%). ¹H NMR (MeOD, 400 MHz) δ (ppm) 7.47 (s, 1H), 7.14 (s, 1H), 4.78 (dd, J = 14.0, 2.0 Hz, 1H), 4.30 (dd, J = 14.0, 8.0 Hz, 1H), 4.15–4.10 (m, 1H), 3.00 (d, J = 11.2 Hz, 1H), 2.91 (d, J = 11.2 Hz, 1H), 2.52 (d, J = 6.4 Hz, 2H), 2.48–2.35 (m, 2H), 2.05 (dd, J = 24.0, 11.6 Hz, 2H), 1.74 (d, J = 11.2 Hz, 2H), 1.42–1.22 (m, 3H); LCMS (ESI) tR: 0.901 min (>99%, ELSD), m/z: 588.1 [M+1]⁺.

HYPOX-2. To a solution of 4 (27 mg, 0.095 mmol) in a mixture of ethanol/dichloromethane (1/2 mL), triethylamine (26 μL, 0.19 mmol) was added, followed by adding Fluorescein isothiocyanate 5 (37 mg, 0.095 mmol). The reaction mixture was heated at 80 °C for 15 min under microwave then cooled to room temperature and concentrated in vacuo. The residue was purified by column chromatography using dichloromethane/MeOH (gradient: 0 to 50% MeOH) to provide HYPOX-2 (49 mg, 76%) as a yellow solid. ¹H NMR (DMSO, 400 MHz) δ (ppm) 8.13 (bs, 1H), 7.72 (d, J = 8.0 Hz, 1H), 7.55 (s, 1H), 7.16 (d, J = 8.0 Hz, 1H), 7.13 (s, 1H), 6.66 (d, J = 2.0 Hz, 2H), 6.60–6.52 (m, 4H), 4.67 (dd, J = 14.0, 3.2 Hz, 1H), 4.20 (dd, J = 14.0, 8.0 Hz, 1H), 4.10–3.95 (m, 1H), 3.42–3.38 (m, 2H), 2.90 (d, J = 10.4 Hz, 1H), 2.77 (d, J = 10.4 Hz, 1H), 2.32–2.20 (m, 2H), 1.99–1.83 (m, 2H), 1.70–1.62 (m, 2H), 1.23–1.01 (m, 3H); LCMS (ESI) tR: 0.901 min (>99%, ELSD), m/z: 588.1 [M+1]⁺.

Animals. C57BL6/J timed pregnant females and adult female mice 5–6 weeks of age were purchased from Charles River Laboratories. All animal experiments were approved by the Vanderbilt University Institutional Animal Care and Use Committee (IACUC).

Mouse Models of Hypoxia for Ex Vivo Imaging. The mouse model of oxygen induced retinopathy (OIR) was selected as a mouse model for hypoxia and generated as published.²⁵ Briefly, litters with 6 to 8 pups were placed into a 75% oxygen chamber with dams from P7–P12. On P12, pups were removed from the hyperoxic environment to room air. Imaging agents, vehicle controls, and dye controls were intravitreally injected (3 μg in 1 μL injection volume) or intravenously injected via tail vein (60 mg/kg) 6 h after removal from hyperoxic environment. Pimonidazole hydrochloride (Hypoxprobe Inc.) was injected intraperitoneally at a concentration of 60 mg/kg body weight.

Cell Culture. Primary human Müller cells and R28 cell line were grown in low glucose DMEM supplemented with 10% Fetal Bovine Serum, 1× GlutaMAX, and 1× Penicillin–Streptomycin. Human Retinal Microvascular Endothelial Cells (HRMEC) were grown in Endothelial Cell Media (EBM) supplemented with EGM SingleQuots Kit. All cells were maintained in a humidified environment with 5% CO₂ at 37 °C unless otherwise noted. For hypoxia induction, assay plates were placed into a humidified chamber and ambient air was displaced with a mixture of 5% CO₂ and 95% N₂ at a flow rate of 20L/min for 5 min according to manufacturer instructions

and published methods.³¹ The chamber was clamped and placed at 37 °C for the remainder of the time point. R28 cells were treated with 100 μM Pimonidazole hydrochloride diluted in complete media and subjected to hypoxia or normoxia for 4 h.

In Vitro Imaging Agent Uptake Assays. R28 cells or primary human Müller cells were seeded at a density of 15,000 cells per well in a 96-well black plate with clear bottom. When 90% confluent, assay plates were either placed in hypoxia or kept in normoxia for 12 h. They were treated with imaging agents diluted in complete media and returned to hypoxia or kept in normoxia for 30 min. They were washed 4 times with prewarmed Hank's Buffered Salt Solution (HBSS), kept in normoxia for 1 h, and then washed 4 more times in HBSS. Fluorescence intensity was read (Absorbance: 490 nm, Emission: 520 nm) using a Synergy Mx Plate Reader from Biotek.

Immunofluorescence Analysis of Cells. R28 cells were seeded at a density of 15,000 cells per well of 8-well chamber slides. When 90% confluent, cells were treated with either imaging agent and Pimonidazole hydrochloride or imaging agent only, diluted in complete media, and placed in hypoxia or normoxia for 4 h. Cells were washed 4 times in HBSS, fixed for 10 min with 10% neutral buffered formalin at room temperature, washed 3 times with tris buffered saline, and mounted with Prolong Gold with DAPI mounting media.

Toxicity Studies. A BrdU cell proliferation assay was performed on R28 cells. The assay was performed according to the manufacturer's protocol with the following specifications. Cells were seeded at 2000 cells/well in a 96-well plate. Twenty-four hours after seeding, the cells were serum starved for 6 h. Imaging agents and vehicle controls diluted in complete media were added and allowed to incubate for 24 h. Four hours prior to the end of the incubation, BrdU was added at a concentration of 10 μM. An Alexa Fluor 647 Click-IT TUNEL in situ detection kit was used on paraffin-embedded retinal sections from adult mice according to manufacturer instructions (Life Technologies). A DNase I treated slide was used as a positive control.

Immunofluorescence Analysis of Retinal Tissues. Retinas were dissected from ocular tissues and fixed in 10% neutral buffered formalin for 2 h. Tissues were then rinsed in Tris buffered saline and blocked/permeabilized in 10% donkey serum with 1% Triton X-100/0.05% Tween 20 in TBS for 6 h. Retinas were then stained for ICAM-2 and Pimonidazole adducts (Hypoxyprobe) followed by secondary antibody staining as indicated. Images were taken using an epifluorescence microscope.

■ ASSOCIATED CONTENT

S Supporting Information

Characterization of HYPOX-1 and -2: NMR, LCMS. Additional figures as described in text. This material is available free of charge via the Internet at <http://pubs.acs.org>.

■ AUTHOR INFORMATION

Corresponding Author

*Phone: (615) 343-7851. E-mail: ash.jayagopal@vanderbilt.edu.

Notes

The authors declare no competing financial interest.

■ ACKNOWLEDGMENTS

This work was supported in part by National Institutes of Health (R01EY23397, P30008126), the American Diabetes Association (7-12-JF-30), the Brightfocus Foundation, the International Retinal Research Foundation, and Research to Prevent Blindness (Unrestricted Grant to Vanderbilt Eye Institute, and a Dolly Green Special Scholar Award (A.J.)).

■ REFERENCES

- (1) Cunha-Vaz, J. G. (2004) The blood-retinal barriers system. Basic concepts and clinical evaluation. *Exp. Eye Res.* 78, 715–21.
- (2) Linsenmeier, R. A., Braun, R. D., McRiley, M. A., Padnick, L. B., Ahmed, J., Hatchell, D. L., McLeod, D. S., and Lutty, G. A. (1998) Retinal hypoxia in long-term diabetic cats. *Invest. Ophthalmol. Vis. Sci.* 39, 1647–57.
- (3) Poulaki, V., Qin, W., Joussen, A. M., Hurlbut, P., Wiegand, S. J., Rudge, J., Yancopoulos, G. D., and Adamis, A. P. (2002) Acute intensive insulin therapy exacerbates diabetic blood-retinal barrier breakdown via hypoxia-inducible factor-1alpha and VEGF. *J. Clin. Invest.* 109, 805–15.
- (4) Grunwald, J. E., Metelitsina, T. I., Dupont, J. C., Ying, G. S., and Maguire, M. G. (2005) Reduced foveolar choroidal blood flow in eyes with increasing AMD severity. *Invest. Ophthalmol. Vis. Sci.* 46, 1033–8.
- (5) Metelitsina, T. I., Grunwald, J. E., DuPont, J. C., and Ying, G. S. (2006) Effect of systemic hypertension on foveolar choroidal blood flow in age related macular degeneration. *Br. J. Ophthalmol.* 90, 342–6.
- (6) Traustason, S., Kiilgaard, J. F., Karlsson, R. A., Hardarson, S. H., Stefansson, E., and la Cour, M. (2013) Spectrophotometric retinal oximetry in pigs. *Invest. Ophthalmol. Vis. Sci.* 54, 2746–51.
- (7) Hardarson, S. H., Elfarsson, A., Agnarsson, B. A., and Stefansson, E. (2013) Retinal oximetry in central retinal artery occlusion. *Acta Ophthalmol.* 91, 189–90.
- (8) Hammer, M., Vilser, W., Riemer, T., and Schweitzer, D. (2008) Retinal vessel oximetry—calibration, compensation for vessel diameter and fundus pigmentation, and reproducibility. *J. Biomed. Opt.* 13, 054015.
- (9) Hardarson, S. H., Harris, A., Karlsson, R. A., Halldorsson, G. H., Kagemann, L., Rechtman, E., Zoega, G. M., Eysteinsson, T., Benediktsson, J. A., Thorsteinsson, A., Jensen, P. K., Beach, J., and Stefansson, E. (2006) Automatic retinal oximetry. *Invest. Ophthalmol. Vis. Sci.* 47, 5011–6.
- (10) Kristjansdottir, J. V., Hardarson, S. H., Harvey, A. R., Olafsdottir, O. B., Eliasdottir, T. S., and Stefansson, E. (2013) Choroidal oximetry with a noninvasive spectrophotometric oximeter. *Invest. Ophthalmol. Vis. Sci.* 54, 3234–9.
- (11) Wanek, J., Teng, P. Y., Blair, N. P., and Shahidi, M. (2013) Inner retinal oxygen delivery and metabolism under normoxia and hypoxia in rat. *Invest. Ophthalmol. Vis. Sci.* 54, 5012–9.
- (12) Dai, C., Liu, X., Zhang, H. F., Puliafito, C. A., and Jiao, S. (2013) Absolute retinal blood flow measurement with a dual-beam Doppler optical coherence tomography. *Invest. Ophthalmol. Vis. Sci.* 54, 7998–8003.
- (13) Ljungkvist, A. S., Bussink, J., Rijken, P. F., Raleigh, J. A., Denekamp, J., and Van Der Kogel, A. J. (2000) Changes in tumor hypoxia measured with a double hypoxic marker technique. *Int. J. Radiat. Oncol. Biol. Phys.* 48, 1529–38.
- (14) Varia, M. A., Calkins-Adams, D. P., Rinker, L. H., Kennedy, A. S., Novotny, D. B., Fowler, W. C., Jr., and Raleigh, J. A. (1998) Pimonidazole: a novel hypoxia marker for complementary study of tumor hypoxia and cell proliferation in cervical carcinoma. *Gynecol. Oncol.* 71, 270–7.
- (15) Arteel, G. E., Thurman, R. G., and Raleigh, J. A. (1998) Reductive metabolism of the hypoxia marker Pimonidazole is regulated by oxygen tension independent of the pyridine nucleotide redox state. *Eur. J. Biochem.* 253, 743–50.
- (16) Nordmark, M., Lancaster, J., Aquino-Parsons, C., Chou, S. C., Ladekarl, M., Havsteen, H., Lindegaard, J. C., Davidson, S. E., Varia, M., West, C., Hunter, R., Overgaard, J., and Raleigh, J. A. (2003)

Measurements of hypoxia using Pimonidazole and polarographic oxygen-sensitive electrodes in human cervix carcinomas. *Radiother. Oncol.* 67, 35–44.

(17) Seigel, G. M. (1996) Establishment of an E1A-immortalized retinal cell culture. *In Vitro Cell. Dev. Biol.: Anim.* 32, 66–8.

(18) Seigel, G. M., Mutchler, A. L., Adamus, G., and Imperato-Kalmar, E. L. (1997) Recoverin expression in the R28 retinal precursor cell line. *In Vitro Cell. Dev. Biol.: Anim.* 33, 499–502.

(19) Capozzi, M. E., McCollum, G. W., and Penn, J. S. (2014) The role of cytochrome P450 epoxygenases in retinal angiogenesis. *Invest. Ophthalmol. Vis. Sci.* 55, 4253–60.

(20) Penn, J. S., Madan, A., Caldwell, R. B., Bartoli, M., Caldwell, R. W., and Hartnett, M. E. (2008) Vascular endothelial growth factor in eye disease. *Prog. Retin. Eye Res.* 27, 331–71.

(21) Yu, S. J., Yoon, J. H., Lee, J. H., Myung, S. J., Jang, E. S., Kwak, M. S., Cho, E. J., Jang, J. J., Kim, Y. J., and Lee, H. S. (2011) Inhibition of hypoxia-inducible carbonic anhydrase-IX enhances hexokinase II inhibitor-induced hepatocellular carcinoma cell apoptosis. *Acta Pharmacol. Sin.* 32, 912–20.

(22) Yaromina, A., Zips, D., Thamess, H. D., Eicheler, W., Krause, M., Rosner, A., Haase, M., Petersen, C., Raleigh, J. A., Quennet, V., Walenta, S., Mueller-Klieser, W., and Baumann, M. (2006) Pimonidazole labelling and response to fractionated irradiation of five human squamous cell carcinoma (hSCC) lines in nude mice: the need for a multivariate approach in biomarker studies. *Radiother. Oncol.* 81, 122–9.

(23) Nordmark, M., Lancaster, J., Chou, S. C., Havsteen, H., Lindegaard, J. C., Davidson, S. E., Varia, M., West, C., Hunter, R., Overgaard, J., and Raleigh, J. A. (2001) Invasive oxygen measurements and Pimonidazole labeling in human cervix carcinoma. *Int. J. Radiat. Oncol. Biol. Phys.* 49, 581–6.

(24) Gass, J. D., Sever, R. J., Sparks, D., and Goren, J. (1967) A combined technique of fluorescein funduscopy and angiography of the eye. *Arch. Ophthalmol.* 78, 455–61.

(25) Smith, L. E., Wesolowski, E., McLellan, A., Kostyk, S. K., D'Amato, R., Sullivan, R., and D'Amore, P. A. (1994) Oxygen-induced retinopathy in the mouse. *Invest. Ophthalmol. Vis. Sci.* 35, 101–11.

(26) Mowat, F. M., Luhmann, U. F., Smith, A. J., Lange, C., Duran, Y., Harten, S., Shukla, D., Maxwell, P. H., Ali, R. R., and Bainbridge, J. W. (2010) HIF-1alpha and HIF-2alpha are differentially activated in distinct cell populations in retinal ischaemia. *PLoS One* 5, e11103.

(27) Mezu-Ndubuisi, O. J., Wanek, J., Chau, F. Y., Teng, P. Y., Blair, N. P., Reddy, N. M., Raj, J. U., Reddy, S. P., and Shahidi, M. (2014) Correspondence of retinal thinning and vasculopathy in mice with oxygen-induced retinopathy. *Exp. Eye Res.* 122, 119–22.

(28) Piao, W., Tsuda, S., Tanaka, Y., Maeda, S., Liu, F., Takahashi, S., Kushida, Y., Komatsu, T., Ueno, T., Terai, T., Nakazawa, T., Uchiyama, M., Morokuma, K., Nagano, T., and Hanaoka, K. (2013) Development of azo-based fluorescent probes to detect different levels of hypoxia. *Angew. Chem., Int. Ed.* 52, 13028–32.

(29) Kiyose, K., Hanaoka, K., Oushiki, D., Nakamura, T., Kajimura, M., Suematsu, M., Nishimatsu, H., Yamane, T., Terai, T., Hirata, Y., and Nagano, T. (2010) Hypoxia-sensitive fluorescent probes for in vivo real-time fluorescence imaging of acute ischemia. *J. Am. Chem. Soc.* 132, 15846–8.

(30) Takahashi, S., Piao, W., Matsumura, Y., Komatsu, T., Ueno, T., Terai, T., Kamachi, T., Kohno, M., Nagano, T., and Hanaoka, K. (2012) Reversible off-on fluorescence probe for hypoxia and imaging of hypoxia-normoxia cycles in live cells. *J. Am. Chem. Soc.* 134, 19588–91.

(31) Dai, Y., Bae, K., and Siemann, D. W. (2011) Impact of hypoxia on the metastatic potential of human prostate cancer cells. *Int. J. Radiat. Oncol. Biol. Phys.* 81, 521–8.